EXPERIMENTAL INVESTIGATIONS ON CAVITATIONS OF MARINE PROPELLERS USING QUANTITATIVE IMAGE-BASED METHODS

Yaw-Huei Lee
Department of Systems Engineering & Naval Architecture, National Taiwan Ocean University, Keelung, Taiwan, R.O.C.

Yi-Chih Chow
Department of Systems Engineering & Naval Architecture, National Taiwan Ocean University, Keelung, Taiwan, R.O.C., ycchow@ntou.edu.tw

Yu-Chi Chang
Department of Systems Engineering & Naval Architecture, National Taiwan Ocean University, Keelung, Taiwan, R.O.C.
Green Energy and Environment Research Laboratories, Industrial Technology Research Institute, Taiwan, R.O.C.

EXPERIMENTAL INVESTIGATIONS ON CAVITATIONS OF MARINE PROPELLERS USING QUANTITATIVE IMAGE-BASED METHODS

Acknowledgements

EXPERIMENTAL INVESTIGATIONS ON CAVITATIONS OF MARINE PROPELLERS USING QUANTITATIVE IMAGE-BASED METHODS

Yaw-Huei Lee[1], Yi-Chih Chow[1], and Yu-Chi Chang[1, 2]

Fig. 1. Sample image of cavitation associated with a marine propeller.

ABSTRACT

Cavitations associated with marine propellers have been a major issue in naval architecture and marine propulsion. Among them, sheet and bubble cavitations are especially impactful in ship propulsion, structural vibration and noise, and propeller damage. Even though numerical simulations are becoming more and more powerful in computing complex flows like cavitating propeller flows, their modelings and resulting data still need to be validated by experiments. Due to the fact that most of the experimental methods for cavitations of marine propellers are only qualitative, this paper develops a quantitative image-based method to extract from cavitation images data useful to the validations of the numerical results. The experimental methodology and setup consist of a phase-locked imaging system incorporated with a dynamometer installed in a cavitation tunnel. Series of images at the same phase for unsteady and quasi-steady sheet cavitations, and bubble cavitation are acquired and then processed and analyzed with different algorisms and procedures developed in light of the respective characteristics of these cavitations. The experimental data provide not only quantitative comparisons, validations, and even calibrations to the numerical modelings and results, but also physical insights such as the correlation of sheet cavitation with propeller dynamics.

I. INTRODUCTION

Marine propellers induce several types of cavitation due to their high rotational speeds and heavy loading conditions that the pressure of the water flowing around them becomes lower than the saturated vapor pressure. Cavitation usually causes vi-brations of ship structure and hence noises, reduces propeller efficiency, and shortens the life span of the propeller. Three types of cavitation are mainly associated with marine propellers: tip vortex cavitation, sheet cavitation and bubble cavitation (Fig. 1). Their causes and effects are described as follows (Carlton, 2012):

(1) Tip vortex cavitation occurs at the center of the rapidly rotating tip vortex where the pressure is very low. The exciting forces and noises resulting from it may cause problems of vibration and noise and even damages to the ship hull.
(2) Sheet cavitation usually appears when the attack angle of the propeller blade increases or the cavitation number decreases. Sheet cavitation often causes thrust breakdown and hence low propeller efficiency.
(3) Bubble cavitation usually starts with small bubble nuclei containing non-condensable gases, flowing through the low pressure area on the blade surface and growing up to large vapor bubbles. It is often found in regions around the middle of the blade chord. Bubble cavitation may enter the high pressure area on the blade surface and collapse, forming high-speed micro jets that impinge on the blade surface to cause erosion phenomenon, a major damage problem to the propeller.

Cavitation effects on marine propellers are mostly detrimental, with few exceptions like super cavitation to reduce the torque experienced by the super-cavitating propeller and sheet cavitation to be used to maintain efficiency over a broad range

of ship speed by the Trans-Velocity Propeller (TVP) (Hwang et al., 2011). As a result, one of the major design objectives for marine propellers is to avoid occurrence of cavitation or at least minimize it. In order to verify the design, cavitation data must be obtained via experimental model tests or numerical simulations. Due to the fact that experimental model tests are costly and time-consuming, numerical simulations become the major tool to not only verify the design, but also contribute to speeding up the design loop. However, numerical simulations themselves need the verification and validation at least in certain benchmark cases. Therefore, qualitative experimental data are still in demand.

Since cavitation poses great engineering challenges to marine propellers, many efforts have been invested in this topic. The majority of them are experimental works, using qualitative methodologies for a quick answer or solution to the cavitation problems. For example, Chen (2008) manually took random image snapshots of cavitation; Konno et al. (2002) used hand-made sketches to illustrate the process of the tip vortex cavitation bursting. However, quantitative data for cavitation problems becomes increasingly demanding recently as mentioned above and these qualitative results are no longer satisfactory. In response to this need, Pereira et al. (2004) started to use digital image processing technique for analyzing their images of a cavitating propeller to quantitatively identify the extension of the sheet cavity area on the propeller surface. More recently, Hu (2010) used the phase-locked imaging technique to collect images of some highly unsteady sheet cavitation occurrences and processed them with several algorithms such as thresholding, linear filtering (Laplacian, Sobel, average), nonlinear filtering (maximum, median, minimum), etc. (see Woods and Gonzalez, 2008). Chang et al. (2010) proposed to quantify cavitation occurrences using the spatial distribution of "cavitation occurrence probability" (COP).

This paper follows Hu (2010) and Chang et al. (2010) to examine the quantitative image-based methodology applied on the cavitation problems associated with marine propellers, particularly focusing on the bubble cavitation. In this paper, image pattern recognition is used, edge detection is improved, and schemes of Morphology are adopted. These efforts enable us to more accurately identify locations, areas, patterns, and occurrence probabilities of cavitations. It is also proposed to categorize the cavitation phenomena of marine propellers into steady-state and unsteady-state and use different methods to analyze respective cavitation images.

EXPERIMENTAL SETUP

In this paper, open water tests and cavitation imaging for marine propellers are conducted in the cavitation tunnel located at the National Taiwan Ocean University. Three model propellers are used in this study as described below:

1. Propeller A

It is a four-bladed propeller with an area ratio of 1.0 and a pitch ratio of 1.4; its foil section is originated from Scherer and

Table 1. Results of the open water test for Propeller B at cavitation imaging conditions of advance coefficient (*J*).

	J	K_T	$10*K_Q$	η_O
1	1.60	0.1123	0.5177	0.5739
2	1.45	0.2057	0.6971	0.6949
3	1.30	0.2205	0.6769	0.6758
4	1.14	0.1590	0.5294	0.5485

Stairs (1994) of US Navy with a design purpose of improving propeller's performance associated with cavitation; the cavitation on its blades can be categorized as unsteady sheet cavitation.

2. Propeller B (Chow, 2009)

It is a four-bladed propeller with a special foil section called "Thrust-Reserved Foil" (TRF) (Hwang, 2012) whose design purpose is to be used to constitute a so-called "Trans-Velocity Propeller" (TVP) (Hwang et al., 2011). The TVP is a fixed-pitch propeller capable of maintaining high-efficiency performances in a broad range of ship speed (about 20-40 knots). Therefore, the complicated, costly controllable pitch propeller can be replaced with the TVP. Propeller B is the first propeller consisting of the TRF whose pressure side is of cambers of opposite signs. This special geometry is to induce certain "appropriate" cavitation on the pressure side of the TVP in order to reduce the torque needed, and hence maintain the efficiency.

Cavitation imaging of Propeller B is performed at four values of advance coefficient (*J*): *J* = 1.60, 1.45, 1.30 and 1.14. Table 1 shows Propeller B's thrust coefficient (K_T), torque coefficient, (K_Q), and efficiency (η_O) at these four *J*'s with definitions as follows:

$$K_T = \frac{T}{\rho \times n^2 \times D^4} \tag{1}$$

$$K_Q = \frac{Q}{\rho \times n^2 \times D^5} \tag{2}$$

$$\eta_o = \frac{J}{2\pi} \frac{K_T}{K_Q} \tag{3}$$

where T denotes the thrust, Q the torque, ρ the water density, n the rotational speed, and D the diameter of the propeller. The cavitation on Propeller B's blades can be categorized as quasi-steady sheet cavitation and bubble cavitation.

3. Propeller C (Chow, 2011)

It is also a four-bladed TVP with a TRF whose design in thickness and chamber is different from that of Propeller B. Fig. 2 shows the *K-J* chart at cavitation number (σ) of 0.55 (corresponding to ship speed of 40 knots) for Propeller C. Cavitation imaging of this propeller is performed at *J* = 1.20, 1.10 and
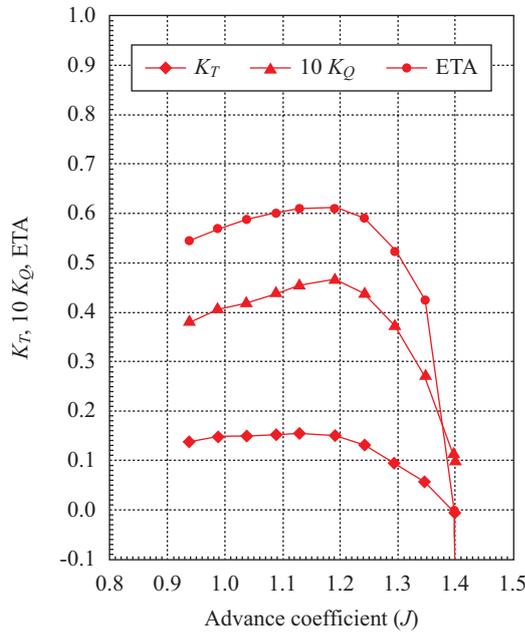
Fig. 2.   Propeller C's *K-J* chart at cavitation number (σ) of 0.55 (corresponding to ship speed of 40 knots).
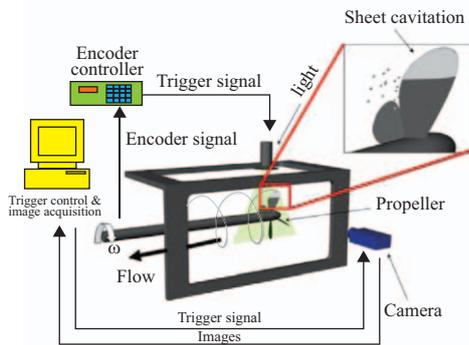
Fig. 3.   Schematic of the experimental setup and cavitation imaging system with signals.

1.00. The cavitation on Propeller C's blades can be categorized as quasi-steady sheet cavitation.

The cavitation imaging system used in this paper includes a LaVision Imager ProX 2M CCD camera which can be externally triggered and whose resolution is 1600×1200 pixel^2, an externally-triggered high-power stroboscope as the light source, and a phase-locked synchronous image acquisition system operated with LaVision's DaVis 7. As shown in Fig. 3, the signal from the encoder of the motor which drives the propeller continuously feeds to the image acquisition system, which analyses the signal to find the timing of a preset phase angle of the propeller and synchronously sends trigger signals to the CCD camera and the stroboscope both for imaging cavitation. Fig. 4 shows the on-site picture of the experimental setup. Series of these phase-locked images acquired by the CCD camera are firstly stored in the camera's memory and then dumped to the
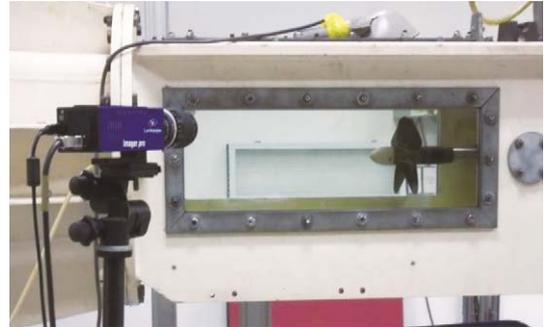
Fig. 4.   On-site picture of the experimental setup.

computer's hard drives for further processing and analysis after the experiment is done. Fig. 1 actually shows a cavitation image sample we acquire using the imaging system described above.

III. CAVITATION IMAGE PROCESSING AND ANALYSIS

As aforementioned, the patterns of cavitation occurring on the blades of the three propellers tested in this study are first inspected visually and then can be categorized into quasi-steady and unsteady sheet cavitations, and (unsteady) bubble cavitation. We develop image processing and analysis techniques corresponding to each of them with MATLAB and its Image Processing Toolbox as follows.

1. Unsteady Sheet Cavitation

The key issues with images of unsteady sheet cavitation are how to separate the cavitation image from the propeller background and enhance it to a complete level for further quantifications. Using Propeller A as an example, the algorithms and procedures are briefly described as follows and more details can be found in Chow et al. (2016):

(a) Subtract the non-cavitating image (only propeller background) from the cavitating image (cavitation + propeller background, as shown in Fig. 5(a) for an example) and perform binarization with certain threshold;

(b) Perform maximum filtering to replace the gray-level value at the center of a image mask with the maximum gray-level value found within the mask. With this step, the holes and discontinuities within the cavitation image obtained from (a) can be filled up or connected;

(c) Perform minimum filtering to replace the gray-level value at the center of a image mask with the minimum gray-level value found within the mask. With this step, the artificial expansion of the cavitation image resulting from (b) can be reduced and restored to its original shape and size.

The image mask of the sheet cavitation is thus obtained. As shown in Fig. 5(b) for an example, the image mask matches the sheet cavitation pretty well. In fact, Chow et al. (2016) estimates the error associated with this procedure to be less than 5%,

(a)

(b)
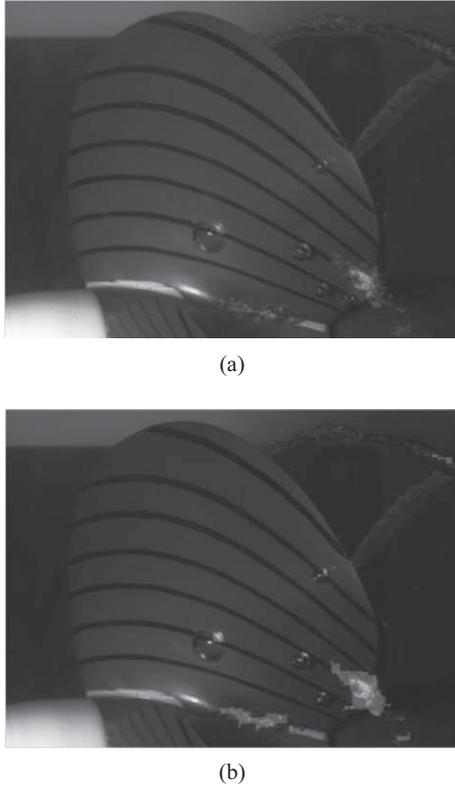
Fig. 5. (a) Propeller A's cavitation image sample, and (b) sheet cavitation image mask superimposed on (a).

| (a) | (b) |
| (c) | (d) |

(e)

Fig. 6. Bubble cavitation image sample processed with the proposed procedure of (a) histogram equalization, (b) Canny edge detection, (c) morphological dilation, (d) morphological erosion, and (e) pattern recognition based on the circularity.

meaning that for any pixel position in the image of the blade, whether it is covered by sheet cavitation or not is identified wrongly in not more than 5 images within 100 images.

With the image results obtained using the procedure described above, a statistical parameter for the occurrence of cavitation, cavitation occurrence probability (COP), can be defined as (Chang et al., 2010)

$$COP(i, j) \equiv \frac{\sum_{n=1}^{N} C_n(i, j)}{N} \qquad (4)$$

where $C_n(i, j)$ is the cavitation indicator for the (i, j) pixel in the nth image that equals 1 if this pixel is covered by cavitation or 0 otherwise. And N is the total number of images. The COP distributions for unsteady cavitations occurring on propeller blades will be discussed later on.

2. (Unsteady) Bubble Cavitation

The image processing and processing technique developed for bubble cavitation is different from the previous one. This is because that bubble cavities appear in a very constant, spherical shape, very different from the rather random shape of unsteady sheet cavitation. Thus, morphological operators (Woods and Gonzalez, 2008) can be used to process this kind of images. For instance, Fig. 1 apparently illustrates two kinds of cavitation

formed on Propeller B: the upper part of quasi-steady sheet cavitation and the bottom part of bubble cavitation. The former is processed by the image-averaging method (as described below) and the latter is processed according to the procedure listed below as well as shown in Fig. 6.

a) Histogram Equalization (Woods and Gonzalez, 2008):

This algorithm is used to enhance the image contrasts for bubbles to be easily identified, as shown for example in Fig. 6(a);

b) Canny Edge Detection (Canny, 1986):

This algorithm is used to detect shapes with high curvature. It uses a first-order Gaussian function to approach the variation of gray scale. Then, a high thresholding is decided to detect the so-called strong edges. Normally, the strong edges are unconnected. A low thresholding is further needed to detect the weak edges. Fig. 6(b) illustrates that our detected edges are still discrete;

c) Morphological Dilation (Woods and Gonzalez, 2008):

This algorithm is used to fill in the space inside as well as between the detected edges in order to solidify the detected bubble. Fig. 6(c) illustrates the clearly detected bubble. However, a dummy tiny bubble is also detected;

d) Morphological Erosion (Woods and Gonzalez, 2008):

This algorithm is used in order to erase the dummy bubble, and the sample result is shown in Fig. 6(d);

e) Pattern Recognition Based on the Circularity:

The circularity is defined as

$$m = \frac{4 \times \pi \times A}{S^2} \qquad (4)$$

where A and S are the area and circumference of the image object detected. The value of m is in-between 0 and 1 corresponding to perfect flatness and perfect roundness, respectively. Through several tests, $m = 0.4$ is appropriate as a threshold to distinguish bubble cavities ($m > 0.4$) from noises ($m < 0.4$). The recognized pattern is shown for example in Fig. 6(e) where two values are labeled: circularity and area.

3. Quasi-Steady Sheet Cavitation

This type of sheet cavitation almost does not change its position, area and shape in time. In other words, the boundary (shape) of this type of cavitation has just small variations in time. So, the time-averaged (or phase-averaged) image of it can be a feasible representation for quasi-steady cavitation, characterizing its position, area and shape. Typically, cavitation images of a time or phase series are first eye-inspected to determine whether it qualifies as quasi-steady cavitation.

The image-averaging method is to produce an averaged image, $P(i, j)$, as follows

$$P(i, j) = \frac{\sum_{n=1}^{N} G_n(i, j)}{N} \qquad (5)$$

where $G_n(i, j)$ is the gray-level value of the pixel coordinates (i, j) on the nth image in a time series or phase series of N images.

IV. RESULTS AND DISCUSSIONS

1. Unsteady Sheet Cavitation

The COP distribution corresponding to Propeller A is shown on the background contours in Figs.7-9 (Chang et al., 2010). It can be observed that the major occurrence of sheet cavitation on the blade of Propeller A is located within 0.4-0.8 r/R, the mid-chord to the trailing edge where COP is above 10%. However, the maximum COP value is below 20%, indicating that the sheet cavitation occurring on Propeller A is strongly unsteady and hence difficult to predict using numerical simulations.

In order to evaluate the predictabilities of numerical models for cavitation with experimental data, Chow et al. (2016) has shown that COP is equivalent to VVF (vapor volume fraction), which is used in RANS (Reynolds Averaged Navier-Stokes Equation Solver) simulations to describe cavitation in an average sense. As a result, RANS simulations with the k-omega SST turbulence model for Propeller A with three cavitation models: Singhal et al. (2002), Zwart et al. (2004) and Schnerr and Sauer (2001), are performed with the commercial CFD software,
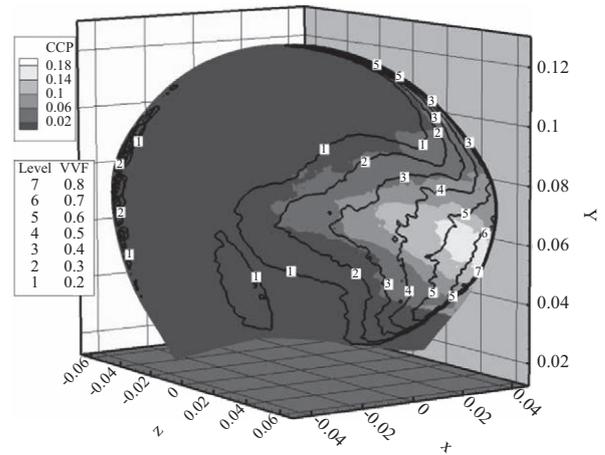
Fig. 7.   Propeller A's VVF distribution resulting from Singhal et al. (2002). The background contour plot shows the experimental COP distribution.
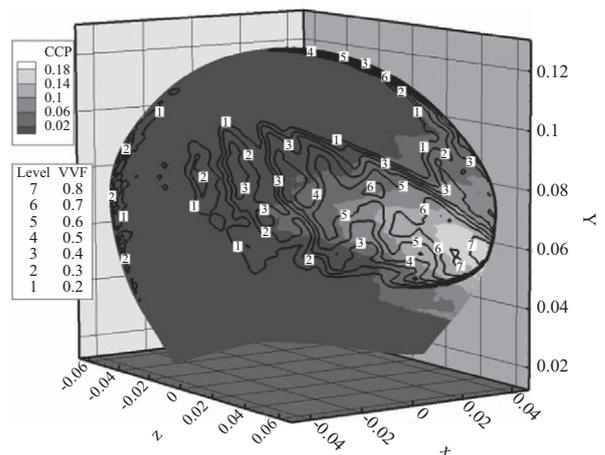
Fig. 8.   Propeller A's VVF distribution resulting from Zwart et al. (2004). The background contour plot shows the experimental COP distribution.
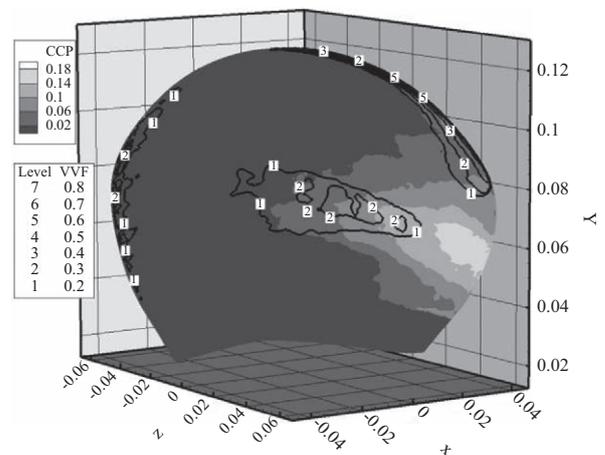
Fig. 9.   Propeller A's VVF distribution resulting from Schnerr and Sauer (2001). The background contour plot shows the experimental COP distribution.
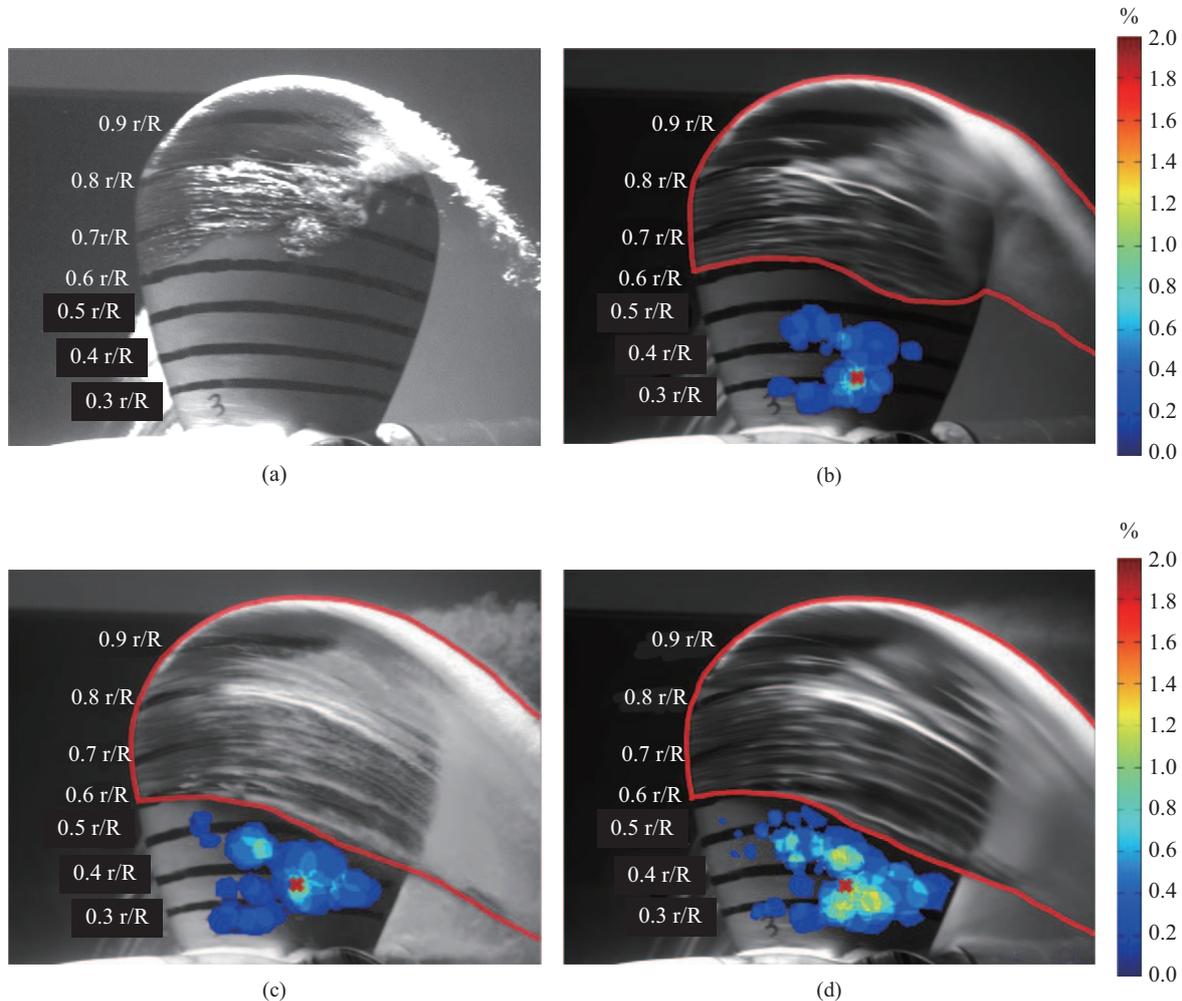
Fig. 10. Averaged images of sheet cavitation and COP distributions of bubble cavitation for Propeller B at *J* = (a) 1.60, (b) 1.45, (c) 1.30 and (d) 1.14.

FLUENT, to obtain three VVF distributions as shown in Figs. 7-9, respectively. Then, correlations of these VVF distributions with the COP one are computed: about 70% for Singhal et al. (2002), about 60% for Zwart et al. (2004), and about 14% for Schnerr and Sauer (2001). Therefore, the cavitation model proposed by Singhal et al. (2002) has better predictability than the other two since its VVF result correlates the experimental COP data better. However, the average VVF values of Figs. 7-9 are obviously much larger than the average COP value on the background, indicating that all the three cavitation models over-predict the amount (occurrences) of sheet cavitation on Propeller A's blade.

2. (Unsteady) Bubble Cavitation

Fig. 10 shows the averaged images of sheet cavitation and the COP distributions of bubble cavitation for Propeller B at *J* = 1.60, 1.45, 1.30 and 1.14. At *J* = 1.60 (Fig. 10(a)), there is only sheet cavitation (no bubble cavitation) occurring on the blade, and this sheet cavitation is not a super-cavitation, i.e., cavity extended beyond the blade. When *J* decreases as the loading of the propeller increases, as clearly shown in Figs. 10(b)-(d),

the coverage area of sheet cavitation increases and develops to super-cavitation; the COP values and occurrence area of bubble cavitation also increase. The red X marks in Figs. 10(b)-(d) indicate the locations of the maximum COP values: Fig. 10(b) (*J* = 1.45), COP_{max} = 1.00% and located at about 0.31 r/R and 0.60 x/C; Fig. 10(c) (*J* = 1.30), COP_{max} = 1.17% and located at about 0.35 r/R and 0.60 x/C; Fig. 10(d) (*J* = 1.14), COP_{max} = 2.50% and located at about 0.34 r/R and 0.58 x/C. It is clearly evident that most bubble cavitation occurs within 0.3-0.5 r/R.

In addition to the COP distributions, other quantification parameters for bubble cavitation can be obtained from the image results. For instance, as shown in Fig. 11, the correlations between bubble cavitation's size (pixel^2) and location (x/C) in different r/R ranges of Propeller B can be deduced to help propeller designers identify the likelihood and possible locations of erosion. It is clearly evident for Propeller B that bubble cavitation mainly locates within 0.4-0.6 x/C; large bubble cavities mainly locate within 0.3-0.4 r/R; large number of bubble cavities mainly locate within 0.4-0.5 r/R. The applications of this kind of data are evidently crucial to the bubble dynamics and numerical simulations associated with the complex pro-
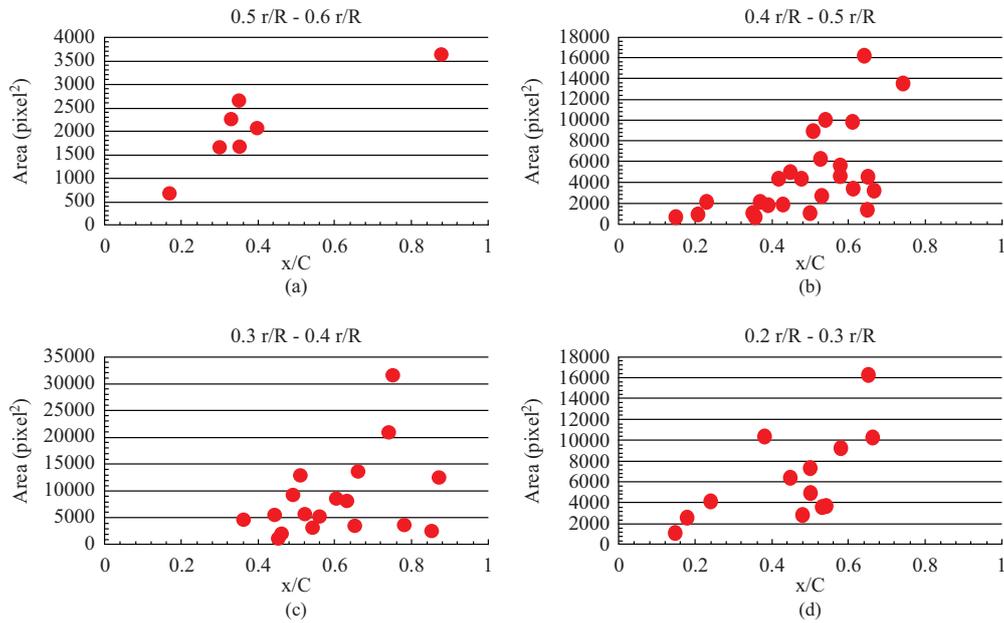
Fig. 11. Correlations between bubble cavitation's size (pixel^2) and location (x/C) in Propeller B's r/R ranges of (a) 0.5-0.6 r/R, (b) 0.4-0.5 r/R, (c) 0.3-0.4 r/R and (d) 0.2-0.3 r/R.
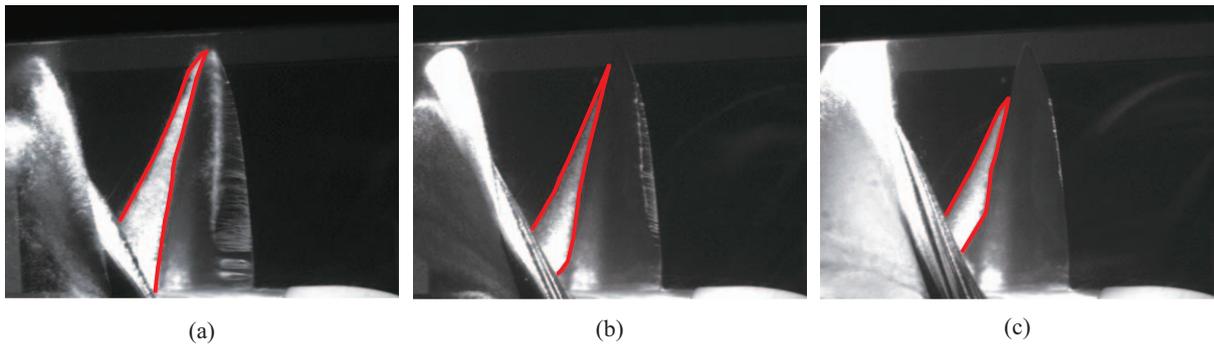
Fig. 12. Averaged cavitation images on the pressure side of Propeller C ($\sigma = 0.55$, corresponding to 40 knots of ship speed) at $J =$ (a) 1.20, (b) 1.10 and (c) 1.00, with bold lines outlining the sheet cavitations upon the area of cambers of opposite signs. The flow direction is from the right to the left.

cesses of occurrence, growth, translation and collapse of bubble cavitation in validations and calibrations of theories and numerical models.

At the application stage, pixel can be converted to physical dimension like meter by mapping the propeller's physical geometry into the 2D image plane (Chow et al., 2016). Due to the scope of this paper and the purpose for clarity, however, pixel is directly used without conversion in the present paper.

3. Quasi-Steady Sheet Cavitation

Due to the fact that the sheet cavitation occurring on the upper part of Propeller B's blade appears to be quasi-steady, the image-averaging method can be applied to characterize its geometry, as already shown with red lines in Fig. 10. It is clearly evident that the area of sheet cavitation on Propeller B gradually increases as the advance coefficient J decreases. This observation corresponds to the K-J data shown in Table 1 where the

growth of the sheet cavitation on the suction side of the blade as J decreases further reduces the thrust to a breakdown level and thus the efficiency η_O.

The same quasi-steady type of sheet cavitation occurs on Propeller C's blade as well. Therefore, the image-averaging method can also be used to process its cavitation images. Fig. 12 shows the averaged cavitation images on the pressure side of Propeller C ($\sigma = 0.55$, corresponding to 40 knots of ship speed) at $J = 1.20$, 1.10 and 1.00 with bold lines outlining the sheet cavitations upon the area of cambers of opposite signs. It is clearly evident that the area of this sheet cavitation decreases as J decreases, indicating that (1) sheet cavitation actually occurs upon the area of cambers of opposite signs as expected; (2) the thrust is actually "reserved" via the decreasing area of the sheet cavitation with the decreasing J (increasing loading). These results are consistent with the K-J chart as shown in Fig. 4. Therefore, cavitation image results combined with the perfor-

mance chart can be regarded as an effective tool to verify the design of propeller.

V. CONCLUDING REMARKS

This paper constructs a phase-locked imaging system and integrates it to a cavitation tunnel for imaging cavitations associated with marine propellers. Image processing and analysis algorithms and procedures are developed corresponding to different cavitation characteristics as follows:

1. Unsteady Sheet Cavitation:

Its image can be mainly processed using combinations of the maximum and minimum filterings to be identified with an image mask. The distribution of cavitation occurrence probability (COP) can thus be obtained and used to compare with the distributions of vapor volume fraction (VVF) resulting from RANS simulations with different cavitation models for validations and evaluations.

2. (Unsteady) Bubble Cavitation:

Its image can be mainly processed using the morphological operators (e.g., dilation and erosion). The location and size data of bubble cavitation as well as the COP distribution can thus be obtained.

3. Quasi-Steady Sheet Cavitation:

Its image can be mainly processed using the image-averaging method. Its image results can be combined with the dynamics data of the propeller (e.g., the K-J chart) to investigate the impacts of cavitation on the performance of the propeller considering its design.

We evaluate three cavitation models (Singhal et al., 2002; Zwart et al., 2004; Schnerr and Sauer, 2001) using the correlations of their respective VVF distributions with the experimental COP data associated with Propeller A and find that the model proposed by Singhal et al. (2002) yields better cavitation results than the other two models. The COP distribution and the location and size data of bubble cavitation resulting from Propeller B are evidently useful in verifying or evaluating the propeller's design as well as validating or calibrating the bubble-dynamics-based cavitation models. The quasi-steady sheet cavitation occurring on the pressure side of Propeller C's blade reduces its area as the advance coefficient J decreases, confirming that the design objectives of this propeller are accomplished.

ACKNOWLEDGEMENTS

REFERENCES

Canny, J. (1986). A computational approach to edge detection. IEEE Transactions on Pattern Analysis and Machine Intelligence, PAMI-8, 6, 679-698.

Carlton, J. S. (2012). Marine Propellers and Propulsion. Oxford: Butterworth-Heinemann.

Chang, Y. C., C. N. Hu, J. C. Tu and Y. C. Chow (2010). Experimental Investigation and Numerical Prediction of Cavitation Incurred on Propeller Surfaces. 9th International Conference on Hydrodynamics, Shanghai, China.

Chen, S. Z. (2008). The influence of propeller root geometries on cavitation pattern at inclined shaft condition. Master Thesis, Department of Systems Engineering and Naval Architecture, National Taiwan Ocean University, Taiwan, Republic of China. (in Chinese)

Chow, Y. C. (2009). Experimental Investigations on the Advanced Propeller Design that Optimizes Performances at Various Ship Speeds (Propeller). Science and Technology Project Final Report: USDDC-740-T452(98R), Ministry of Economic Affairs, R.O.C. (in Chinese, with English Abstract)

Chow, Y. C. (2011). Experimental Investigations on the Performance and Cavitation Characteristics of the Trans-Velocity Propeller Operating at Inclined-Shaft Conditions. Science and Technology Project Final Report: USDDC-1012-T155(100), Ministry of Economic Affairs, R.O.C. (in Chinese, with English Abstract)

Chow, Y. C., Y. H. Lee and Y. C. Chang (2016). Image-Based Measurements for Examining Model Predictability of Cavitation on a Marine Propeller Surface. (submitted to Ocean Engineering)

Hu, C. H. (2010). Experimental Investigation and Analysis of Sheet Cavitations and Wakes Associated with Marine Propellers., Master Thesis, Department of Systems Engineering and Naval Architecture, National Taiwan Ocean University, Taiwan, Republic of China. (in Chinese, with English Abstract)

Hwang, J. L., S. S. Chin, K. K. Chang and C. C. Tu (2011). Development of the Trans-Velocity Propellers. in Second International Symposium on Marine Propulsors.

Hwang, J. L. (2012). Thrust-Reserved Foil & Its Application to the Trans-Velocity Propeller. Advanced Maritime Engineering Conference.

Konno, A., K. Wakabayashi, H. Yamaguchi, M. Maeda, N. Ishii, S. Soejima and K. Kimura (2002). On the Mechanism of the Bursting Phenomena of Propeller Tip Vortex Cavitation. Journal of Marine Science and Technology 6, 181-192.

Pereira, F., F. Salvatore and F. D. Felice (2004). Measurement and Modeling of Propeller Cavitation in Uniform Inflow. Journal of Fluids Engineering 126, 671-679.

Scherer, O. and R. Stairs (1994). Propeller blade sections with improved cavitation performance. the Propellers/Shafting '94 Symposium, Virginia Beach, Virginia, U.S.A.

Schnerr, G. H. and J. Sauer (2001). Physical and numerical modeling of unsteady cavitation dynamics. In Fourth International Conference on Multiphase Flow, New Orleans, U.S.A.

Singhal, A. K., M. M. Athavale, H. Li and Y. Jiang (2002). Mathematical basis and validation of the full cavitation model. Journal of Fluids Engineering, 124, 617-624.

Woods, R. E. and R. C. Gonzalez (2008). Digital Image Processing. PEARSON.

Zwart, P. J., A. G. Gerber and T. Belamri (2004). A two-phase flow model for predicting cavitation dynamics. In Fifth International Conference on Multiphase Flow, Yokohama, Japan.